Journal of Materials Chemistry A

ROYAL SOCIETY OF CHEMISTRY

PAPER

View Article Online
View Journal | View Issue

Cite this: J. Mater. Chem. A, 2020, 8, 5572

Charge transfer dynamics in a singlet fission organic molecule and organometal perovskite bilayer structure†

Deqiang Guo,[a] Lin Ma, *[a] Zilin Zhou,[a] Dabin Lin,[a] Cheng Wang,[a] Xin Zhao,[a] Fangteng Zhang,[a] Jiahua Zhang [b] and Zhaogang Nie*[a]

Received 7th October 2019
Accepted 15th February 2020

DOI: 10.1039/c9ta11022d

rsc.li/materials-a

Carrier dynamics between singlet fission molecules and a perovskite were studied using transient absorption measurements on TIPS-pentacene/$CH_3NH_3PbI_3$ ($MAPbI_3$) bilayer, pristine $MAPbI_3$ and TIPS-pentacene films. Ultrafast electron transfer within 1.5 ps is verified to proceed directly from the correlated bound triplet pair states of TIPS-pentacene generated by a singlet fission process to the $MAPbI_3$ conduction band. Hole transfer from $MAPbI_3$ to TIPS-pentacene proceeds on a much longer time scale of tens of ns. Our study not only unveils the charge carrier dynamics in a singlet fission molecule/perovskite bilayer structure, but also provides new insights on the design of singlet fission sensitized perovskite solar cells with enhanced performance.

Introduction

Organic–inorganic hybrid perovskites, possessing the advantages of low-cost, high absorption coefficients, long carrier diffusion lengths and high charge carrier mobilities, have been extensively studied in the field of photovoltaics in the past few years.[1–3] The record power conversion efficiency (PCE) of a perovskite based single-junction solar cell has reached 25.2%,[4] approaching its theoretical Shockley–Queisser limit (~30.5%).[5] Perovskite solar cells (PSCs) are typically composed of a mesoscopic or planar perovskite layer as a light absorber, sandwiched between an electron transport layer (ETL) and a hole transport layer (HTL). To date, most ETL materials are inorganic metal oxides including TiO_2 and SnO_2, which require a high temperature sintering or annealing process,[6,7] and the most widely used HTL material is 2,2′,7,7′-tetrakis-(*N*,*N*-dip-methoxyphenylamine)-9,9′-spirobifluorene (spiro-MeOTAD) which exhibits a high conductivity after doping.[8,9] Recently, there have been some reports on utilizing novel dopant-free organic molecular semiconductors as HTL or ETL materials in PSCs with enhanced device performances. For instance, pentacene,[10] TIPS-PEN,[11] perylene[10] and tetracene[12] were employed as HTL materials in PSCs with improved device stability and PCE. Several groups applied perylene diimides (PDIs) as ETL layers in PSCs and obtained a higher efficiency compared with that of traditional TiO_2 ETL based devices.[13–15] One common property of these organic molecules arouses our interest, that is, they all undergo a singlet fission (SF) process in a film or a crystalline structure.[16–20] Are these SF molecules only working as HTLs or ETLs in PSCs? Is singlet fission involved in carrier dynamics in a perovskite/SF molecule bilayer structure?

Singlet fission (SF), an exciton multiplication process in organic semiconductors which converts one singlet exciton into two triplet excitons, is a promising way to reduce thermalization loss and circumvent the Shockley–Queisser limit in conventional single-junction solar cells.[21] TIPS-pentacene (6,13-bis(-triisopropylsilylethynyl)pentacene), abbreviated as TIPS-PEN hereafter, is one of the most widely studied SF prototype materials, with SF proceeding on a sub ps time scale in a polycrystalline film.[17,22,23] Kazim *et al.* fabricated TIPS-PEN/$MAPbI_3$/TiO_2 based solar cells with 11.8% efficiency, and suggested TIPS-PEN works as a HTL to receive holes from the $MAPbI_3$ perovskite.[11] Later on, Lee *et al.* studied the carrier dynamics in a TIPS-PEN/$MAPbI_3$ bilayer film and proposed that there is electron transfer from triplet states generated by SF in TIPS-PEN to the $MAPbI_3$ perovskite.[24] Therefore, the carrier dynamics in the TIPS-PEN/$MAPbI_3$ bilayer structure is still ambiguous up till now.

In this work, we studied the charge transfer dynamics between a SF molecule and a perovskite by performing transient absorption (TA) spectroscopic measurements on pristine $MAPbI_3$, TIPS-PEN, and TIPS-PEN/$MAPbI_3$ bilayer films. A fast conversion process (1.5 ps) was observed between the correlated triplet pairs of TIPS-PEN and $MAPbI_3$, and indicates that ultrafast electron transfer occurs from the correlated triplet pair states generated *via* SF in TIPS-PEN to the $MAPbI_3$ perovskite. Time-resolved PL measurements suggest that hole transfer

[a]School of Physics and Optoelectronic Engineering, Guangdong University of Technology, Guangzhou, China. E-mail: malin@gdut.edu.cn; zgnie@gdut.edu.cn
[b]State Key Laboratory of Luminescence and Applications, CIOMP, Chinese Academy of Sciences, Changchun, China

† Electronic supplementary information (ESI) available. See DOI: 10.1039/c9ta11022d

from $MAPbI_3$ to TIPS-PEN proceeds on a time scale of tens of ns. Our study unveils the carrier dynamics in the TIPS-PEN/perovskite bilayer structure, and explores important perspectives of utilizing singlet fission sensitizers to improve the PSC performance.

Results and discussion

To minimize the impact of inhomogeneity from film to film, we fabricated $MAPbI_3$, TIPS-PEN and their interfacial bilayer structures on the same glass substrate using a sequential two-step spin-coating procedure described in Fig. 1a. The detailed fabrication procedure can be found in the Experimental section. The thickness of the $MAPbI_3$ or TIPS-PEN layer is around 85 nm, characterized using the cross-sectional SEM image (Fig. 1b). It is worthy of note that this film is relatively thin compared to those of the practical perovskite solar cells owing to the large extinction coefficient of $MAPbI_3$, since a nonopaque sample is desired in order to obtain the TA spectra in a broad spectral range. The steady-state absorption spectra of $MAPbI_3$, TIPS-PEN and their interfacial bilayer are plotted in Fig. 1c, consistent with previous reports.[2,17,24] The absorption band at 700 nm in the TIPS-PEN layer is indicative of good film crystallinity.[25]

To reveal the ultrafast charge carrier dynamics in the TIPS-PEN/$MAPbI_3$ bilayer film, we performed femtosecond transient absorption (TA) spectroscopy measurements with a broad probe wavelength range (470–1000 nm). First, 800 nm was employed as the pump wavelength to excite $MAPbI_3$ and TIPS-PEN/$MAPbI_3$ layers. In this case, the $MAPbI_3$ perovskite is selectively excited since TIPS-PEN has a higher HUMO–LUMO energy gap and does not absorb at 800 nm (Fig. 1c blue curve). The obtained TA spectral features are similar in both $MAPbI_3$ (Fig. 2a) and TIPS-PEN/$MAPbI_3$ (Fig. 2b), showing the representative TA spectra of $MAPbI_3$, featuring a ground state bleaching (GSB) band at 750 nm and a photoinduced absorption (PIA) band at around 695 nm.[2] Compared with pristine $MAPbI_3$, the GSB spectral feature between the 800 and 900 nm region is missing in TIPS-PEN/$MAPbI_3$, which can be attributed to the reduction of surface and grain boundary defects *via* introducing the organic molecules (TIPS-PEN) into the perovskite layer during spin-coating.[26,27] Apart from this, no new TA bands are observed in TIPS-PEN/$MAPbI_3$. The TA kinetics in $MAPbI_3$ and TIPS-PEN/$MAPbI_3$ show a negligible difference within 6 ns (Fig. 2c), with detailed fitting parameters listed in Table S1 (ESI†). It suggests that the morphology of the $MAPbI_3$ was not dramatically modified by spin-coating TIPS-PEN on top, and we can neglect the effect of surface passivation or additional trap states induced by spin-coating TIPS-PEN on top of $MAPbI_3$.

Next, we performed TA measurements under excitation at 650 nm in order to excite TIPS-PEN. In this scenario, both $MAPbI_3$ and TIPS-PEN were excited. The obtained TA spectra of the pristine $MAPbI_3$ film are shown in Fig. 3a, and are similar to the TA spectra under 800 nm excitation (Fig. 2a). There are three main features in the TA spectra of the TIPS-PEN film (Fig. 3b): (i) two GSB bands at 585 and 700 nm, corresponding well to the steady-state absorption spectrum (Fig. 1c); (ii) a PIA band at around 530 nm due to absorption from triplet states generated *via* a singlet fission process ($T_1 \rightarrow T_n$);[23,28,29] (iii) a broad NIR PIA band at around 860 nm spanning the spectral region from 735 to 1000 nm. There were only a few studies reported on this NIR

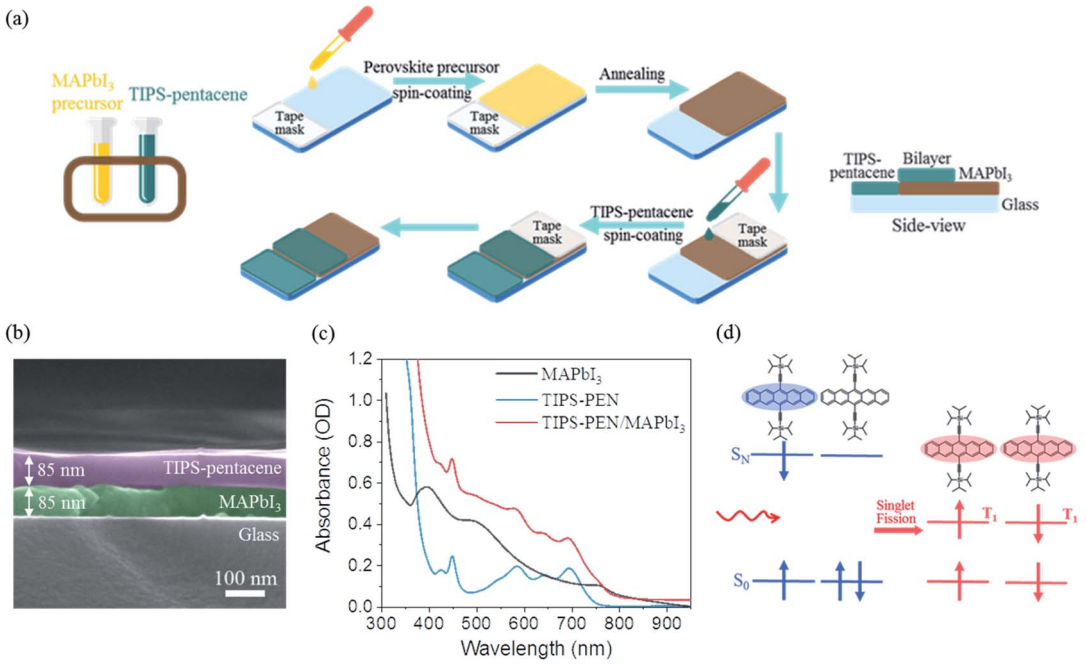

Fig. 1 (a) Schematic illustration of the TIPS-PEN/$MAPbI_3$ bilayer film fabrication process. (b) Cross-sectional SEM image of the TIPS-PEN/$MAPbI_3$ bilayer film. (c) Steady-state absorption spectra of TIPS-PEN (blue), $MAPbI_3$ (black) and TIPS-PEN/$MAPbI_3$ (red) films. (d) Scheme for the mechanism of singlet fission in TIPS-PEN.

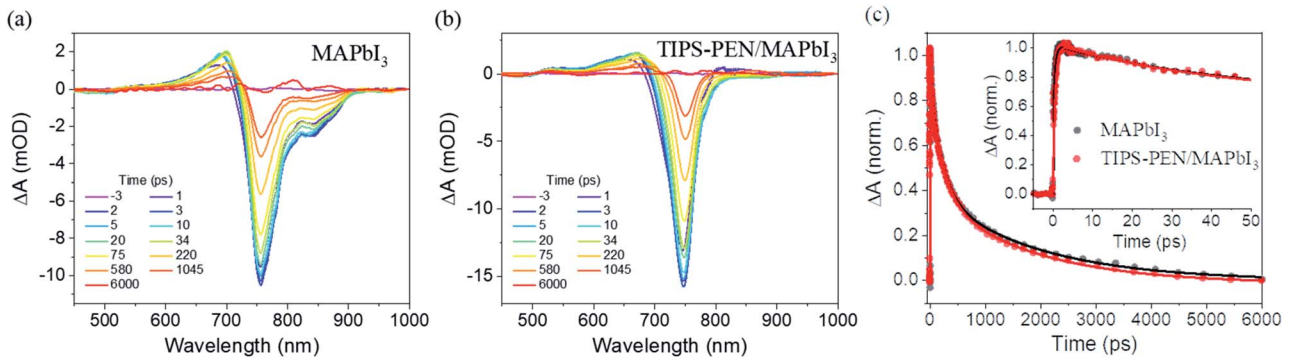

Fig. 2 Transient absorption spectra under excitation at 800 nm of (a) $MAPbI_3$ and (b) TIPS-PEN/$MAPbI_3$ bilayer films at different delay times. (c) Normalized transient kinetics for $MAPbI_3$ (gray) and TIPS-PEN/$MAPbI_3$ bilayer (red) films at 750 nm. Inset: The decay profiles over a shorter time interval of 50 ps.

TA band due to the limited spectral bandwidth. Moreover, the origin of this NIR TA band is still disputable. Yost *et al.*[30] and Herz *et al.*[23] proposed that this TA band was due to $T_1 \rightarrow T_2$ transition, while Yong *et al.*[31] and Stuart *et al.*[32] attributed this TA band to the absorption of the correlated bound triplet pair ^{1}(TT) which does not dissociate into two free triplet states. The TA spectra of the TIPS-PEN/$MAPbI_3$ bilayer film under 650 nm excitation (Fig. 3c) contain TA spectral features from both $MAPbI_3$ and TIPS-PEN. Normalized TA kinetics at 735 nm in $MAPbI_3$ and TIPS-PEN/$MAPbI_3$ are plotted in Fig. 3d for comparison. The reason for choosing 735 nm is because it is not only within the GSB band of $MAPbI_3$, but also a quasi-isosbestic point in the TA spectra of TIPS-PEN (Fig. 3b), *i.e.*, the TA signal intensity from TIPS-PEN does not vary much with delay times. Therefore, we choose to compare the $MAPbI_3$ TA kinetics at 735 nm in $MAPbI_3$ and TIPS-PEN/$MAPbI_3$ to rule out the influence from TIPS-PEN. As shown in Fig. 3d, there is an additional rise time component of 1.49 ± 0.04 ps, obtained from fitting the results for the TIPS-PEN/$MAPbI_3$ bilayer compared to the pristine $MAPbI_3$ film. Furthermore, the relaxation lifetime also becomes longer in the TIPS-PEN/$MAPbI_3$ bilayer. The TA kinetics in a 5 ns time window (Fig. 3d–f), together with the detailed fitting parameters are shown in Fig. S1 and Table S2 (ESI†). These differences indicate that there is either charge or

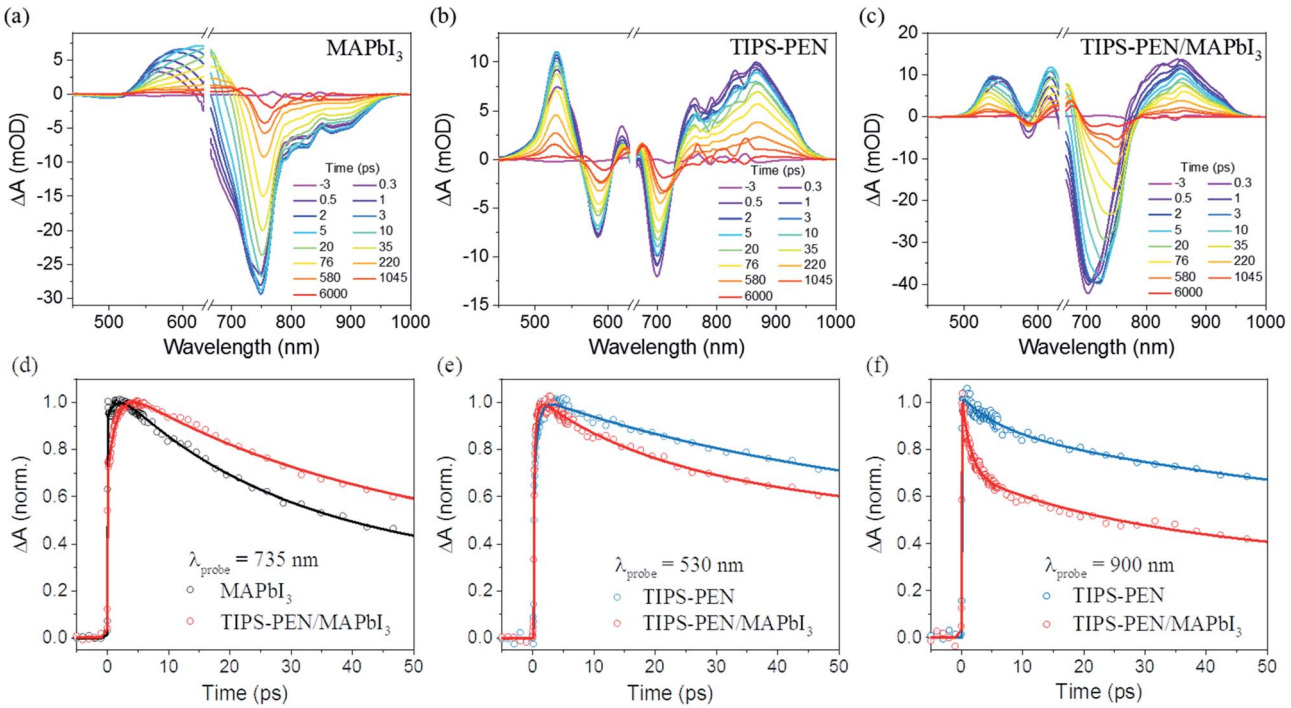

Fig. 3 Transient absorption spectra under excitation at 650 nm of (a) $MAPbI_3$, (b) TIPS-PEN and (c) TIPS-PEN/$MAPbI_3$ bilayer films at different delay times (the excitation scattering at around 650 nm was removed for clarity). (d)–(f) Normalized transient kinetics of $MAPbI_3$ (black), TIPS-PEN (blue) and the TIPS-PEN/$MAPbI_3$ bilayer (red) at different probe wavelengths.

energy transfer from excited TIPS-PEN to $MAPbI_3$ proceeding on an ultrafast ps time scale in the TIPS-PEN/$MAPbI_3$ bilayer film. It is known that the TIPS-PEN film undergoes ultrafast (~100 fs) singlet fission which converts the excited singlet state S_1 into two triplet states T_1.[33–35] The energy of T_1 (0.85 eV (ref. 36 and 37)) in TIPS-PEN is much lower than the bandgap of $MAPbI_3$ (~1.6 eV), if energy transfer occurs, it would be expected to originate from S_1 to $MAPbI_3$ and should be fast enough to compete with the SF. Furthermore, energy transfer, either Dexter or resonant energy transfer (RET), is known to result in an excited state in the acceptor. In the case of the TIPS-PEN/$MAPbI_3$ bilayer, energy transfer from TIPS-PEN to $MAPbI_3$ will result in an increase of electron and hole densities in $MAPbI_3$. It is known that free carriers (electrons and holes) are generated in the $MAPbI_3$ perovskite upon photoexcitation.[38] Therefore, the carrier dynamics in $MAPbI_3$ follows the second order recombination model, *i.e.*, $dN/dt \propto -kN_eN_h$. It means that the higher the carrier density, the faster the carrier recombination. Therefore, we would expect the TA kinetics of $MAPbI_3$ becomes shortened if energy transfer occurs from TIPS-PEN to $MAPbI_3$ due to the increase of electron and hole densities. However, Fig. 3d suggests that the TA kinetics of $MAPbI_3$ became slightly slower rather than shortened in the bilayer structure compared to the pristine $MAPbI_3$ film. It indicates that energy transfer from TIPS-PEN to $MAPbI_3$ is not the dominant carrier relaxation pathway in the TIPS-PEN/$MAPbI_3$ bilayer after photoexcitation.

It is known that energy level matching is a criterion for efficient charge transfer. As reported previously, the highest occupied molecular orbital (HOMO) and the lowest unoccupied molecular orbital (LUMO) energies of TIPS-PEN in the solid state depend on the film thickness.[39] Therefore, it is necessary to precisely determine the energy levels of TIPS-PEN and $MAPbI_3$ layers employed in our study. UPS measurements were then carried out. The HOMO energy of the TIPS-PEN layer was determined to be −5.06 eV from the UPS spectrum (Fig. S2a, ESI†). The lower bound for the lowest unoccupied molecular orbital (LUMO) energy of −3.35 eV was calculated by adding the HOMO–LUMO gap obtained from the $(\alpha h\nu)^2 - h\nu$ plot (Fig. S2b, ESI†). Similarly, the valence and conduction band energies of $MAPbI_3$ were determined to be −5.46 and −3.95 eV, respectively (Fig. S2, ESI†), in agreement with a previous report.[40] The energy level of TIPS-PEN triplet states is estimated by adding the triplet energy of pentacene 0.85 eV (ref. 36 and 37) to the HOMO level. Regarding the energy level of ^{1}(TT), previous literature reported that the ^{1}(TT) state is nearly iso-energetic with S_1 or twice energy of T_1 in materials with high SF efficiencies.[41,42] Therefore, we use the energy of $2E(T_1)$ to represent the energy level of ^{1}(TT) in the TIPS-PEN film. Based on the above, the energy level diagram of the TIPS-PEN/$MAPbI_3$ bilayer is plotted in Fig. 4b. It can be seen that the triplet state energy level is ill-suited for charge transfer to the $MAPbI_3$ conduction band (endothermic by ~0.25 eV). Therefore, we can expect that the charge transfer from triplet states of TIPS-PEN to the conduction band of $MAPbI_3$ will not be efficient. The other possible charge transfer path is electron transfer from the correlated bound triplet pair state (denoted by ^{1}(TT) hereafter) generated *via* SF in TIPS-PEN to the $MAPbI_3$ conduction band. This charge transfer route is further

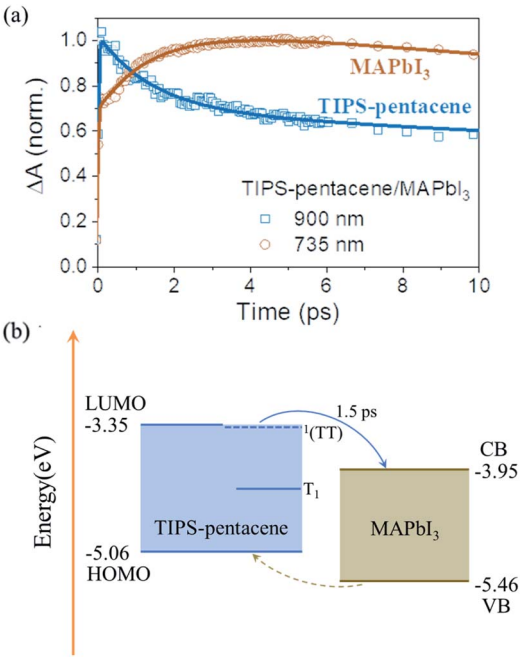

Fig. 4 (a) Normalized transient kinetics of $MAPbI_3$ (black) and TIPS-PEN (blue) in the TIPS-PEN/$MAPbI_3$ bilayer film. (b) Energy-level diagram of the TIPS-PEN/$MAPbI_3$ bilayer film.

confirmed in our study by comparing the TA kinetics at λ_{probe} = 900 nm and was attributed to ^{1}(TT) states of TIPS-PEN.[31,32] As shown in Fig. 3f, the lifetime of the ^{1}(TT) state in the TIPS-PEN/$MAPbI_3$ bilayer is much shortened compared to the pristine TIPS-PEN film. Detailed fitting results are summarized in Table S2 (ESI†). The first decay component $\tau_1 = 1.50 \pm 0.09$ ps of the ^{1}(TT) state (λ_{probe} = 900 nm) is in excellent agreement with the rise time component $\tau_0 = 1.49 \pm 0.04$ ps obtained for TA kinetics of $MAPbI_3$ (λ_{probe} = 735 nm) in the TIPS-PEN/$MAPbI_3$ bilayer. A more straightforward comparison of the two TA kinetics is shown in Fig. 4a. Therefore, we conclude that ultrafast electron transfer proceeds from the correlated triplet pair state generated *via* SF in TIPS-PEN to the $MAPbI_3$ conduction band on a time scale of ps, as shown in Fig. 4b (solid blue arrow). In Fig. 3e, the TA kinetics at 530 nm in TIPS-PEN/$MAPbI_3$ also shows a slight shortening compared to pristine TIPS-PEN, in agreement with a previous report.[24] We assign this to the charge transfer from the long-lived S_1 or T_n states generated by triplet–triplet annihilation (TTA) in TIPS-PEN to the $MAPbI_3$ conduction band. It is also possibly due to the spectral overlap between ^{1}(TT) and T_1 in the visible range since it is always difficult to completely separate the spectral features of T_1 and ^{1}(TT). However, it is noteworthy that this charge transfer route is much less efficient compared to the direct triplet pair charge transfer route mentioned above. Lee *et al.* also observed the NIR TA band in the TIPS-PEN film, however, with a much lower amplitude.[24] This weak NIR band was fully covered by the negative GSB signal from $MAPbI_3$ in the bilayer structure. In our study, the NIR TA band is much more pronounced. We believe the main origin of this difference is from the morphology variations of the TIPS-PEN layer. In ref. 24,

the bilayer film was heated at 60 °C for 1 hour after depositing TIP-PEN on top of $MAPbI_3$. We annealed the TIPS-PEN film at 80 °C for 1 h, which results in a more ordered TIPS-PEN film which favours the formation of a triplet pair state and allows observing the ultrafast CT channel from ^{1}(TT) to $MAPbI_3$. Direct multielectron transfer from the ^{1}(TT) state has been reported previously.[31,37,43,44] The first reported system is the pentacene/C_{60} bilayer by Zhu *et al.* through a time-resolved two photon photoemission spectroscopy study, which suggests that two-electron transfer (2ET) from ^{1}(TT) of pentacene to C_{60} occurs in 400 fs and dominates the relaxation pathway, whereas one-electron transfer (1ET) from free triplets proceeds on a longer timescale.[37] A follow up study reported that tetracene also undergoes 2ET from the ^{1}(TT) state to C_{60} but with much lower efficiency.[43] In our study, the TA kinetics in the TIPS-PEN/$MAPbI_3$ bilayer suggests that direct two-electron transfer (2ET) from ^{1}(TT) of TIPS-PEN to $MAPbI_3$ is the most plausible dominant electron transfer pathway. Since if only one-electron transfer (1ET) occurs from ^{1}(TT), one triplet state will be left as a product after 1ET.[37] Therefore, we would expect to observe a rise component of ~1.5 ps in the T_1 kinetics which corresponds to the ultrafast decay of ^{1}(TT). However, as shown in Fig. 3e, there is no visible additional rise component in the T_1 kinetics in the TIPS-PEN/$MAPbI_3$ bilayer. In order to mimic the practical working conditions of a solar cell under illumination with broad solar spectrum, broadband excitation TA spectra were also measured, shown in Fig. S3 (ESI†). The fitting results are presented in Table S3 (ESI†). Similar to the results obtained under narrowband excitation at 650 nm, the electron transfer from ^{1}(TT) to $MAPbI_3$ proceeds within 1 ps.

There was no detectable steady-state photoluminescence (PL) in the TIPS-PEN film,[45] due to the efficient PL quenching by the ultrafast singlet fission process. Therefore, as shown in Fig. 5a, the steady-state PL spectra of $MAPbI_3$ and TIPS-PEN/$MAPbI_3$ only show the PL signature from $MAPbI_3$, centered at around 775 nm.[2] Furthermore, under identical experimental conditions, the PL intensity of $MAPbI_3$ is apparently reduced when interfaced with the TIPS-PEN layer. Moreover, the PL lifetime of the TIPS-PEN/$MAPbI_3$ bilayer is also shortened compared with the pristine $MAPbI_3$ layer (Fig. 5b), with fitted average lifetimes of 28.3 ns and 9.3 ns for $MAPbI_3$ and TIPS-PEN/$MAPbI_3$, respectively. Detailed fitting parameters of the time-resolved PL traces are shown in Table S4 (ESI†). The PL intensity decrease or lifetime shortening of $MAPbI_3$ in the TIPS-PEN/$MAPbI_3$ bilayer is expected to originate from either charge or energy transfer from $MAPbI_3$ to TIPS-PEN. The transfer time can be estimated to be around 13.8 ns using the equation: $1/\tau_0 + 1/\tau_{transfer} = 1/\tau_1$, where τ_0 is the original PL lifetime in the pristine perovskite film (28.3 ns), and τ_1 is the PL lifetime of the bilayer film (9.3 ns). As mentioned previously, the carrier dynamics in $MAPbI_3$ follows the second order recombination model, *i.e.*, $dN/dt \propto -kN_eN_h$.[46] The ultrafast electron transfer from TIPS-PEN to $MAPbI_3$ will increase the electron density, thus, enhance the carrier recombination, resulting in a shorter PL lifetime in $MAPbI_3$. However, as shown in Fig. 4a and Table S2 (ESI†), the amplitude percentage of a 1.4 ps rise component in the TA kinetics of $MAPbI_3$ is about 38%. Thus, we can estimate the electron density in $MAPbI_3$ increases by 38% due to electron transfer from ^{1}(TT) of TIPS-PEN to $MAPbI_3$. However, this could not explain why the PL lifetime is shortened by 3 times and the steady state PL intensity shows an apparent decrease. The other possible reason is that charge or energy transfer takes place from $MAPbI_3$ to TIPS-PEN. The energy level alignment in Fig. 4b shows that hole transfer is energetically favoured than electron or energy transfer from $MAPbI_3$ to TIPS-PEN. Kazim *et al.* fabricated solar cells using TIPS-PEN as a hole transporting layer with a PCE of 11.8%.[11] Nienhaus *et al.* recently reported that $MA_{0.15}FA_{0.85}PbI_3$ thin films can function as efficient triplet sensitizers of rubrene through sequential electron and hole transfer, with a triplet sensitization rate of τ = 15 ns.[47] This transfer rate agrees well with our extracted PL quenching rate (13.8 ns), which indicates that besides hole transfer to the HOMO of TIPS-PEN, electrons could also possibly transfer to TIPS-PEN to form a bound triplet, and delayed PL from TIPS-PEN could be expected *via* a triplet–triplet annihilation (TTA) process. However, as mentioned above, except for the PL feature from $MAPbI_3$, we did not observe any visible shorter PL emission which could be attributed to TIPS-PEN in the steady state PL spectra. Therefore, it is unlikely that triplet sensitization could be the dominant PL quenching channel investigated here. Therefore, we attribute the $MAPbI_3$ PL quenching to hole transfer from $MAPbI_3$ to TIPS-PEN, with a transfer rate of around 13.8 ns. It is noteworthy that this hole transfer is much slower than that reported in the $MAPbI_3$/spiro-OMeTAD heterostructure (0.75 ns).[2] However, Kazim *et al.* reported a higher PCE (11.8%) and a short-circuit current density J_{sc} (20.84 mA cm^{-2}) using the $MAPbI_3$/TIPS-PEN based device than the PCE (9.77%) and J_{sc} (18.61 mA cm^{-2}) of $MAPbI_3$/spiro-OMeTAD based device.[11] It indicates that except for hole transfer, there is another channel which increases the carrier density thus enhancing the current density and device efficiency. It could be possibly explained by the ultrafast electron transfer from ^{1}(TT) of TIPS-PEN *via* SF to the $MAPbI_3$ perovskite in our study. In SF based photovoltaic blends, charge transfer can occur from triplet pair states with >100% photon-to-charge conversion efficiency.[31] Utilizing the exciton multiplication merit of SF, thermalization energy loss in conventional single junction perovskite solar cells can be reduced. Therefore, it is

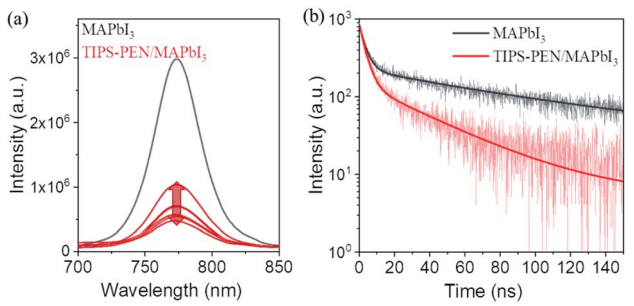

Fig. 5 Time-resolved PL decay curves at 770 nm of $MAPbI_3$ (black), and TIPS-PEN/$MAPbI_3$ bilayer (red) films under excitation at 573 nm (a.u., arbitrary units). The multiple red lines in (a) are PL spectra recorded at different spots in the bilayer film.

highly promising that SF molecules could be applied as sensitizers to further improve the efficiency of perovskite solar cells towards breaking the Shockley–Queisser limit.

Conclusions

To summarize, we performed an extensive spectroscopic study to elucidate the carrier transfer behavior in a TIPS-pentacene/$MAPbI_3$ perovskite heterojunction film. We demonstrated that singlet fission (SF) is involved in the carrier dynamics in the TIPS-pentacene/$MAPbI_3$ bilayer structure. Ultrafast electron transfer is verified to directly proceed from the correlated triplet pair states of TIPS-pentacene generated by SF to the $MAPbI_3$ conduction band within 1.5 ps. Hole transfer from $MAPbI_3$ to TIPS-pentacene proceeds on a much longer time scale of tens of ns. The results observed in this study may also apply to other SF sensitized photovoltaic devices. Future work exploring different SF molecules for fine tuning their energy levels and optimizing the thickness of the SF layer is desired to improve the charge transfer efficiency towards highly efficient SF sensitized photovoltaics.

Experimental section

Materials

Methylammonium iodide (CH_3NH_3I, MAI) and lead iodide (PbI_2) powders were purchased from Xi'an Polymer Light Technology Corp (purity >99%). TIPS-PEN (purity >99%, HPLC grade) was purchased from Ossila Ltd. Anhydrous DMF was purchased from Sigma-Aldrich. Chlorobenzene (purity >99.5%) was purchased from Macklin. All chemicals were used as received without further purification unless otherwise stated.

Sample preparation

The $MAPbI_3$ precursor solution was prepared by dissolving 28.6 mg MAI and 77 mg PbI_2 (1 : 1 molar ratio) in 1 mL anhydrous DMF, resulting in a precursor solution with a concentration of 10 wt%. TIPS-PEN was dissolved in chlorobenzene with a concentration of 40 mg mL^{-1}. The $MAPbI_3$ precursor solution and the TIPS-PEN solution were stirred at 70 °C until all components were fully dissolved. Glass substrates were cleaned using the Hellmanex III solution (1%) and isopropanol solution in an ultrasonication system for 5 min respectively, sequentially dried with a compressed air gun, and then cleaned with ultraviolet/ozone treatment for 30 min.

The $MAPbI_3$, TIPS-PEN and TIPS-PEN/$MAPbI_3$ bilayer films were fabricated on a single glass substrate using a sequential two-step spin-coating procedure described in Fig. 1a. One third of the glass substrate was first covered using masking tape (Scotch 810, 3M) and then spin-coated with the $MAPbI_3$ precursor (4000 rpm). After removing the masking tape, the glass was transferred to a hot plate for annealing at 80 °C for 30 min until the film colour turned from yellow into dark brown, resulting in two-thirds of the glass covered with $MAPbI_3$. Half of the $MAPbI_3$ film was covered with another masking tape and sequentially spin-coated with TIPS-PEN on top (3000 rpm). After detaching the masking tape, the obtained film was finally annealed on the hot plate at 80 °C for 10 min to remove the residual solvent. The whole fabrication procedure was conducted in a nitrogen filled glove box. The sample was used as is without intentional encapsulation. After spin-coating, we performed the optical characterization immediately on the as-fabricated film. The as-fabricated film could survive around 3–5 days under our lab conditions with a constant temperature of 23 °C and a humidity of 35%. The tape mask does not influence the properties of the $MAPbI_3$ layer, as demonstrated in Fig. S4 (ESI†). In addition, the oxygen quenching effect on the triplet states can be ruled out due to the low triplet energy of TIPS-PEN (0.85 eV, significantly lower than the transition energy of triplet oxygen → singlet oxygen). It is further confirmed by the TA measurements on the TIPS-PEN film stored in a vacuum using an Optistat DN-V2 optical cryostat (Oxford Instruments) and in air as shown in Fig. S5 (ESI†).

Steady-state characterization

The cross-sectional (SEM) image of the TIPS-PEN/$MAPbI_3$ bilayer film was recorded using a Hitachi SU8220 field emission microscope operated at 10 kV. The steady-state absorption spectra were measured with a Shimadzu UV 3600 Plus spectrometer. The steady-state PL spectra were recorded using a Fluorolog 3 spectrofluorometer (HORIBA Jobin Yvon) under excitation at 600 nm. To minimize the scattering or other influence on the excitation light intensity, for all optical characterization, we illuminated the sample from the $MAPbI_3$ side, *i.e.*, from the glass substrate side for both single layer or bilayer structures.

Ultraviolet photoelectron spectroscopy (UPS)

The UPS spectra were recorded using an X-ray Photoelectron Spectrometer/ESCA (ESCALAB 250Xi, Thermo Fisher Scientific). The measurements were performed in a multi-chamber ultra-high vacuum system with a base pressure of 5×10^{-10} mbar, using He I (21.22 eV) with a resolution of 10 meV. To obtain the secondary electron cut-off (SEC), a sample bias of −5 V was applied in the normal emission geometry. The Fermi level edge of a sputtered clean Au film was measured to calibrate all UPS spectra and used to define the reference zero binding energy.

Time-resolved photoluminescence

Time-resolved PL measurements were performed using the time-correlated single-photon counting (TCSPC) module of a Fluorolog 3 spectrofluorometer. The excitation light source is a pulsed laser diode (570 nm, 1 MHz repetition rate). The overall time resolution is 1.6 ns as determined from the deconvolution of the instrument response function (IRF).

Transient absorption (TA) spectroscopy

The TA spectra were collected using an amplified Ti:sapphire laser system (Solstice Ace, Spectra Physics), with an output of 800 nm at a 1 kHz repetition rate, a 35 fs pulse width, and a power of 6 W. Broadband pulses (470–1000 nm) are produced

by spectrally broadening the output 800 nm pulse in a neon-filled hollow-core fiber. Pulse compression by the chirped mirrors yields a pulse width of 8 fs. The broadband pulses were split into two beams using a beamsplitter. The weaker one was used as a probe beam, and the stronger one was used as the broadband excitation pump beam. The 650 nm pump pulse is selectively generated by inserting a bandpass filter (center at 650 nm, 10 nm bandwidth) into the original broadband pump pulse path. 800 nm excitation TA experiments were performed using the fundamental output from the amplifier as a pump pulse. The probe pulses were generated by focusing 800 nm pulses on a 3 mm sapphire window to generate white light continuum. A pump fluence of 650 nm is 283 μJ cm^{-2} (50 fs, 1 kHz) and an excitation fluence of 800 nm is 566 μJ cm^{-2} (50 fs, 1 kHz). A computer-controlled, piezo-driven high precision translation stage (Physik Instrumente) incorporated with a long travel range motorized stage (Newport) was placed in the pump beam arm to generate a time delay between pump and probe pulses with a 1 fs time delay precision and a 8 ns time window.

Conflicts of interest

There are no conflicts to declare.

Acknowledgements

This work was supported by the National Natural Science Foundation of China (grant no. 11874125, 11704079, and 11774071), the Science and Technology Program of Guangzhou (grant no. 201804010451 and 201904010104), the State Key Laboratory of Luminescence and Applications (grant no. SKLA-2019-08), and the Guangdong University Students Science and Technology Innovation Training Special Fund (grant no. pdjh2019b0155).

References

1 S. D. Stranks, G. E. Eperon, G. Grancini, C. Menelaou, M. J. P. Alcocer, T. Leijtens, L. M. Herz, A. Petrozza and H. J. Snaith, *Science*, 2013, **342**, 341–344.
2 G. Xing, N. Mathews, S. Sun, S. S. Lim, Y. M. Lam, M. Gratzel, S. Mhaisalkar and T. C. Sum, *Science*, 2013, **342**, 344–347.
3 M. Gratzel, *Nat. Mater.*, 2014, **13**, 838–842.
4 NREL Efficiency Chart, *This plot is courtesy of the National Renewable Energy Laboratory*, Golden, CO, available online: https://www.nrel.gov/pv/assets/pdfs/best-research-cell-efficiencies.20190802.pdf, accessed on 07 Aug 2019.
5 L. M. Pazos-Outón, T. P. Xiao and E. Yablonovitch, *J. Phys. Chem. Lett.*, 2018, **9**, 1703–1711.
6 H. Zhou, Q. Chen, G. Li, S. Luo, T.-b. Song, H.-S. Duan, Z. Hong, J. You, Y. Liu and Y. Yang, *Science*, 2014, **345**, 542–546.
7 J. P. Correa Baena, L. Steier, W. Tress, M. Saliba, S. Neutzner, T. Matsui, F. Giordano, T. J. Jacobsson, A. R. Srimath Kandada, S. M. Zakeeruddin, A. Petrozza, A. Abate, M. K. Nazeeruddin, M. Grätzel and A. Hagfeldt, *Energy Environ. Sci.*, 2015, **8**, 2928–2934.
8 M. Liu, M. B. Johnston and H. J. Snaith, *Nature*, 2013, **501**, 395–398.
9 J. Burschka, N. Pellet, S.-J. Moon, R. Humphry-Baker, P. Gao, M. K. Nazeeruddin and M. Grätzel, *Nature*, 2013, **499**, 316.
10 X. Zhang, M. Li, C. Dall'Agnese, G. Chen, X.-F. Wang and T. Miyasaka, *Dyes Pigm.*, 2019, **160**, 285–291.
11 S. Kazim, F. J. Ramos, P. Gao, M. K. Nazeeruddin, M. Grätzel and S. Ahmad, *Energy Environ. Sci.*, 2015, **8**, 1816–1823.
12 M. Abdi-Jalebi, M. Ibrahim Dar, S. P. Senanayak, A. Sadhanala, Z. Andaji-Garmaroudi, L. M. Pazos-Outón, J. M. Richter, A. J. Pearson, H. Sirringhaus, M. Grätzel and R. H. Friend, *Sci. Adv.*, 2019, **5**, eaav2012.
13 H. Zhang, L. Xue, J. Han, Y. Q. Fu, Y. Shen, Z. Zhang, Y. Li and M. Wang, *J. Mater. Chem. A*, 2016, **4**, 8724–8733.
14 J.-l. Wu, W.-K. Huang, Y.-C. Chang, B.-C. Tsai, Y.-C. Hsiao, C.-Y. Chang, C.-T. Chen and C.-T. Chen, *J. Mater. Chem. A*, 2017, **5**, 12811–12821.
15 D. Zou, F. Yang, Q. Zhuang, M. Zhu, Y. Chen, G. You, Z. Lin, H. Zhen and Q. Ling, *ChemSusChem*, 2019, **12**, 1155–1161.
16 P. M. Zimmerman, Z. Zhang and C. B. Musgrave, *Nat. Chem.*, 2010, **2**, 648–652.
17 C. Ramanan, A. L. Smeigh, J. E. Anthony, T. J. Marks and M. R. Wasielewski, *J. Am. Chem. Soc.*, 2011, **134**, 386–397.
18 L. Ma, K. J. Tan, H. Jiang, C. Kloc, M.-E. Michel-Beyerle and G. G. Gurzadyan, *J. Phys. Chem. A*, 2014, **118**, 838–843.
19 J. J. Burdett, A. M. Müller, D. Gosztola and C. J. Bardeen, *J. Chem. Phys.*, 2010, **133**, 144506.
20 S. W. Eaton, L. E. Shoer, S. D. Karlen, S. M. Dyar, E. A. Margulies, B. S. Veldkamp, C. Ramanan, D. A. Hartzler, S. Savikhin, T. J. Marks and M. R. Wasielewski, *J. Am. Chem. Soc.*, 2013, **135**, 14701–14712.
21 M. B. Smith and J. Michl, *Chem. Rev.*, 2010, **110**, 6891–6936.
22 A. J. Musser, M. Liebel, C. Schnedermann, T. Wende, T. B. Kehoe, A. Rao and P. Kukura, *Nat. Phys.*, 2015, **11**, 352.
23 J. Herz, T. Buckup, F. Paulus, J. Engelhart, U. H. F. Bunz and M. Motzkus, *J. Phys. Chem. Lett.*, 2014, **5**, 2425–2430.
24 S. Lee, D. Hwang, S. I. Jung and D. Kim, *J. Phys. Chem. Lett.*, 2017, **8**, 884–888.
25 M. J. Y. Tayebjee, K. N. Schwarz, R. W. MacQueen, M. Dvořák, A. W. C. Lam, K. P. Ghiggino, D. R. McCamey, T. W. Schmidt and G. J. Conibeer, *J. Phys. Chem. C*, 2016, **120**, 157–165.
26 D. Wei, F. Ma, R. Wang, S. Dou, P. Cui, H. Huang, J. Ji, E. Jia, X. Jia, S. Sajid, A. Elseman, L. Chu, Y. Li, B. Jiang, J. Qiao, Y. Yuan and M. Li, *Adv. Mater.*, 2018, **30**, 1707583.
27 C. Liu, Z. Huang, X. Hu, X. Meng, L. Huang, J. Xiong, L. Tan and Y. Chen, *ACS Appl. Mater. Interfaces*, 2018, **10**, 1909–1916.
28 C. Grieco, G. S. Doucette, R. D. Pensack, M. M. Payne, A. Rimshaw, G. D. Scholes, J. E. Anthony and J. B. Asbury, *J. Am. Chem. Soc.*, 2016, **138**, 16069–16080.
29 J. Herz, T. Buckup, F. Paulus, J. U. Engelhart, U. H. F. Bunz and M. Motzkus, *J. Phys. Chem. A*, 2015, **119**, 6602–6610.
30 S. R. Yost, J. Lee, W. B. WilsonMark, T. Wu, D. P. McMahon, R. R. Parkhurst, N. J. Thompson, D. N. Congreve, A. Rao, K. Johnson, M. Y. Sfeir, M. G. Bawendi, T. M. Swager,

R. H. Friend, M. A. Baldo and T. Van Voorhis, *Nat. Chem.*, 2014, **6**, 492–497.
31 C. K. Yong, A. J. Musser, S. L. Bayliss, S. Lukman, H. Tamura, O. Bubnova, R. K. Hallani, A. Meneau, R. Resel, M. Maruyama, S. Hotta, L. M. Herz, D. Beljonne, J. E. Anthony, J. Clark and H. Sirringhaus, *Nat. Commun.*, 2017, **8**, 15953.
32 A. N. Stuart, P. C. Tapping, E. Schrefl, D. M. Huang and T. W. Kee, *J. Phys. Chem. C*, 2019, **123**, 5813–5825.
33 J. Herz, T. Buckup, F. Paulus, J. Engelhart, U. H. Bunz and M. Motzkus, *J. Phys. Chem. Lett.*, 2014, **5**, 2425–2430.
34 A. J. Musser, M. Liebel, C. Schnedermann, T. Wende, T. B. Kehoe, A. Rao and P. Kukura, *Nat. Phys.*, 2015, **11**, 352–357.
35 C. Y. Wong, B. L. Cotts, H. Wu and N. S. Ginsberg, *Nat. Commun.*, 2015, **6**, 5946.
36 M. Rei Vilar, M. Heyman and M. Schott, *Chem. Phys. Lett.*, 1983, **94**, 522–526.
37 W.-L. Chan, M. Ligges, A. Jailaubekov, L. Kaake, L. Miaja-Avila and X.-Y. Zhu, *Science*, 2011, **334**, 1541–1545.
38 J. S. Manser and P. V. Kamat, *Nat. Photonics*, 2014, **8**, 737–743.
39 O. L. Griffith, J. E. Anthony, A. G. Jones and D. L. Lichtenberger, *J. Am. Chem. Soc.*, 2010, **132**, 580–586.
40 H.-S. Kim, C.-R. Lee, J.-H. Im, K.-B. Lee, T. Moehl, A. Marchioro, S.-J. Moon, R. Humphry-Baker, J.-H. Yum, J. E. Moser, M. Gratzel and N.-G. Park, *Sci. Rep.*, 2012, **2**, 591.
41 N. R. Monahan, D. Sun, H. Tamura, K. W. Williams, B. Xu, Y. Zhong, B. Kumar, C. Nuckolls, A. R. Harutyunyan, G. Chen, H.-L. Dai, D. Beljonne, Y. Rao and X. Y. Zhu, *Nat. Chem.*, 2016, **9**, 341.
42 E. A. Margulies, C. E. Miller, Y. Wu, L. Ma, G. C. Schatz, R. M. Young and M. R. Wasielewski, *Nat. Chem.*, 2016, **8**, 1120–1125.
43 W.-L. Chan, J. R. Tritsch and X. Y. Zhu, *J. Am. Chem. Soc.*, 2012, **134**, 18295–18302.
44 H. Kim, B. Keller, R. Ho-Wu, N. Abeyasinghe, R. J. Vázquez, T. Goodson and P. M. Zimmerman, *J. Am. Chem. Soc.*, 2018, **140**, 7760–7763.
45 A. D. Platt, J. Day, S. Subramanian, J. E. Anthony and O. Ostroverkhova, *J. Phys. Chem. C*, 2009, **113**, 14006–14014.
46 S. D. Stranks, V. M. Burlakov, T. Leijtens, J. M. Ball, A. Goriely and H. J. Snaith, *Phys. Rev. Appl.*, 2014, **2**, 034007.
47 L. Nienhaus, J.-P. Correa-Baena, S. Wieghold, M. Einzinger, T.-A. Lin, K. E. Shulenberger, N. D. Klein, M. Wu, V. Bulović, T. Buonassisi, M. A. Baldo and M. G. Bawendi, *ACS Energy Lett.*, 2019, **4**, 888–895.